

Low-lying dipole resonance in neutron-rich Ne isotopes

Kenichi Yoshida^{1,2} and Nguyen Van Giai²

¹*Department of Physics, Graduate School of Science, Kyoto University, Kyoto 606-8502, Japan*

²*Institut de Physique Nucléaire, IN2P3-CNRS, and Université Paris-Sud, F-91406 Orsay Cedex, France*

(Dated: August 14, 2021)

Microscopic structure of the low-lying isovector dipole excitation mode in neutron-rich ^{26,28,30}Ne is investigated by performing deformed quasiparticle-random-phase-approximation (QRPA) calculations. The particle-hole residual interaction is derived from a Skyrme force through a Landau-Migdal approximation. We have obtained the low-lying resonance in ²⁶Ne at around 8.5 MeV. It is found that the isovector dipole strength at $E_x < 10$ MeV exhausts about 6.0% of the classical Thomas-Reiche-Kuhn dipole sum rule. This excitation mode is composed of several QRPA eigenmodes, one is generated by a $\nu(2s_{1/2}^{-1}2p_{3/2})$ transition dominantly, and the other mostly by a $\nu(2s_{1/2}^{-1}2p_{1/2})$ transition. The neutron excitations take place outside of the nuclear surface reflecting the spatially extended structure of the $2s_{1/2}$ wave function. In ³⁰Ne, the deformation splitting of the giant resonance is large, and the low-lying resonance is overlapping with the giant resonance.

PACS numbers: 21.10.Re; 21.60.Ev; 21.60.Jz

I. INTRODUCTION

The study of nuclei far off stability is one of the most active research fields in nuclear physics [1, 2, 3], and exploring the collective motions unique in unstable nuclei is one of the main issues experimentally and theoretically [4]. In neutron-rich nuclei, because of the absence of the Coulomb barrier the surface structure is quite different from stable nuclei. One of the unique structures is the neutron skin [5, 6]. Since the collective excitations are sensitive to the surface structure, one can expect new kinds of exotic excitation modes associated with the neutron skin to appear in neutron-rich nuclei. One of the examples is the soft dipole excitation [7], which is observed not only in light halo nuclei [8, 9, 10, 11, 12, 13, 14, 15, 16, 17], but also in heavier systems [18, 19, 20], where an appreciable $E1$ strength is observed above the neutron threshold exhausting several percents of the energy-weighted sum rule (EWSR).

The structure of the low-lying dipole state and its collectivity has been studied in the framework of the mean-field calculations by many groups [21, 22, 23, 24, 25, 26, 27, 28, 29, 30, 31, 32, 33]. A low-lying dipole state in neutron-rich ²⁶Ne was first predicted by using the relativistic quasiparticle-random-phase approximation (QRPA) in Ref. [32], and recently it was observed at RIKEN around 9 MeV, exhausting about 5% of the Thomas-Reiche-Kuhn (TRK) dipole sum rule [34]. In Ref. [32], the QRPA was solved in the response function formalism. This method can treat the excitations to the continuum exactly by employing the Green's functions satisfying the out-going-wave boundary conditions, but an additional procedure is required to obtain the microscopic structure of the excitation mode [35].

In the present paper, we investigate the microscopic structure of the low-lying dipole resonance in neutron-rich Ne isotopes, and we discuss the isotopic dependence with special attention to the deformation effects. To this end, we have developed a deformed QRPA code in

the matrix formulation based on the coordinate-space Skyrme-Hartree-Fock-Bogoliubov (HFB) theory.

The paper is organized as follows: In Sec. II, we explain our method. In Sec. III, we check the results of our new calculation scheme by comparing the existing QRPA results. In Sec. IV, we present the results of the deformed QRPA and we discuss the microscopic structure of the low-lying dipole state in ^{26,28,30}Ne. Finally, we summarize the paper in Sec. V.

II. MODEL

We briefly summarize here our approach (see Ref. [36] for details). In order to discuss simultaneously effects of nuclear deformation and pairing correlations including the continuum, we solve the HFB equations [37, 38]

$$\begin{pmatrix} h^\tau(\mathbf{r}\sigma) - \lambda^\tau & \tilde{h}^\tau(\mathbf{r}\sigma) \\ \tilde{h}^\tau(\mathbf{r}\sigma) & -(h^\tau(\mathbf{r}\sigma) - \lambda^\tau) \end{pmatrix} \begin{pmatrix} \varphi_{1,\alpha}^\tau(\mathbf{r}\sigma) \\ \varphi_{2,\alpha}^\tau(\mathbf{r}\sigma) \end{pmatrix} = E_\alpha \begin{pmatrix} \varphi_{1,\alpha}^\tau(\mathbf{r}\sigma) \\ \varphi_{2,\alpha}^\tau(\mathbf{r}\sigma) \end{pmatrix} \quad (1)$$

directly in the cylindrical coordinates assuming axial and reflection symmetries. Here, $\tau = \nu$ (neutron) and π (proton), and $\mathbf{r} = (\rho, z, \phi)$. For the mean-field Hamiltonian h , we employ the SkM* interaction [39]. Details for expressing the densities and currents in the cylindrical coordinate representation can be found in Refs. [40, 41]. The pairing field is treated by using the density-dependent contact interaction [42, 43],

$$v_{pp}(\mathbf{r}, \mathbf{r}') = V_0 \frac{1 - P_\sigma}{2} \left[1 - \left(\frac{\varrho^{\text{IS}}(\mathbf{r})}{\varrho_0} \right)^\gamma \right] \delta(\mathbf{r} - \mathbf{r}'). \quad (2)$$

with $V_0 = -390 \text{ MeV} \cdot \text{fm}^2$ and $\varrho_0 = 0.16 \text{ fm}^{-3}$, $\gamma = 1$. Here, $\varrho^{\text{IS}}(\mathbf{r})$ denotes the isoscalar density and P_σ the spin exchange operator. The pairing strength V_0 is determined so as to approximately reproduce the experimental

pairing gap of 1.25 MeV in ^{28}Ne obtained by the three-point formula [44]. Because the time-reversal symmetry and reflection symmetry with respect to the $x - y$ plane are assumed, we have only to solve for positive Ω and positive z . We use the lattice mesh size $\Delta\rho = \Delta z = 0.6$ fm and the box boundary condition at $\rho_{\text{max}} = 9.9$ fm and $z_{\text{max}} = 9.6$ fm. The quasiparticle energy is cut off at 60 MeV and the quasiparticle states up to $\Omega^\pi = 13/2^\pm$ are included.

Using the quasiparticle basis obtained by solving the HFB equation (1), we solve the QRPA equation in the matrix formulation [45]

$$\sum_{\gamma\delta} \begin{pmatrix} A_{\alpha\beta\gamma\delta} & B_{\alpha\beta\gamma\delta} \\ B_{\alpha\beta\gamma\delta} & A_{\alpha\beta\gamma\delta} \end{pmatrix} \begin{pmatrix} X_{\gamma\delta}^\lambda \\ Y_{\gamma\delta}^\lambda \end{pmatrix} = \hbar\omega_\lambda \begin{pmatrix} 1 & 0 \\ 0 & -1 \end{pmatrix} \begin{pmatrix} X_{\alpha\beta}^\lambda \\ Y_{\alpha\beta}^\lambda \end{pmatrix}. \quad (3)$$

The residual interaction in the particle-particle (p-p) channel appearing in the QRPA matrices A and B is the density-dependent contact interaction (2). On the other hand, for the residual interaction in the particle-hole (p-h) channel, we employ the Landau-Migdal (LM) approximation [46] applied to the density-dependent Skyrme forces [47, 48],

$$v_{ph}(\mathbf{r}, \mathbf{r}') = N_0^{-1} \{ F_0 + F'_0 \boldsymbol{\tau} \cdot \boldsymbol{\tau}' + (G_0 + G'_0 \boldsymbol{\tau} \cdot \boldsymbol{\tau}') \boldsymbol{\sigma} \cdot \boldsymbol{\sigma}' \} \delta(\mathbf{r} - \mathbf{r}'). \quad (4)$$

Here, N_0 is the density of states and the Landau parameters are deduced from the same Skyrme force which generates the mean field. Because the full self-consistency between the static mean-field calculation and the dynamical QRPA calculation is broken, we have to renormalize the residual interaction in the particle-hole channel by an overall factor f_{ph} to get the spurious $K^\pi = 0^-$ or 1^- modes (representing the center-of-mass motion) at zero energy ($v_{ph} \rightarrow f_{ph} \cdot v_{ph}$). We cut the two-quasiparticle space at $E_\alpha + E_\beta \leq 60$ MeV due to the excessively demanding computer memory as well as the calculation time if we used a model space consistent with that adopted in the HFB calculation. Accordingly, we need another factor f_{pp} for the particle-particle channel. We determine this factor such that the spurious $K^\pi = 0^+$ mode associated with the particle number fluctuation appears at zero energy ($v_{pp} \rightarrow f_{pp} \cdot v_{pp}$).

III. CHECK OF THE CALCULATION SCHEME

In this section, we compare our results with those of Ref. [49]. In this reference, the SLy4 interaction [50] for the mean field and the surface-type delta interaction with $\gamma = 1.5$ and $V_0 = -415.73 \text{ MeV} \cdot \text{fm}^3$ for the pairing field were employed for the HFB calculation, and the quasiparticle energy was cut off at 50 MeV. Therefore, we adopt these parameters for the comparisons in this section. The differences between the present calculation and that in Ref. [49] are the mesh size, the boundary condition, the cutoff energy for the QRPA calculation,

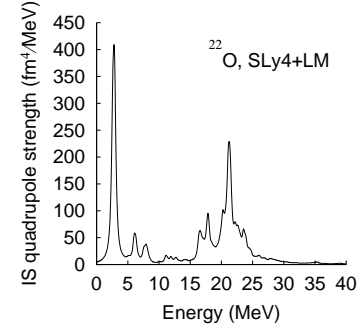


FIG. 1: Response function for the isoscalar quadrupole operator in ^{22}O . The transition strengths are smeared by using a Lorentzian function with a width of $\Gamma = 0.5$ MeV. The renormalization factors for the QRPA calculation are $f_{ph} = 0.982$, $f_{pp} = 1.18$. The cutoff energy is 60 MeV.

and the treatment of the spin-dependent interaction (G_0 and G'_0) in Eq. (4). In the present calculation, the spin transition density is treated exactly.

In Fig. 1, we show the isoscalar quadrupole response function in ^{22}O . The first 2^+ state is located at 2.8 MeV with $B(E2 \uparrow) = 18.9 e^2\text{fm}^4$. The experimental values are $E(2^+)_{\text{exp}} = 3.2$ MeV and $B(E2)_{\text{exp}} = 21 \pm 8 e^2\text{fm}^4$ [51, 52, 53]. In Ref. [49], the energy and the transition strength are $E(2^+) = 1.9$ MeV and $B(E2) = 22 e^2\text{fm}^4$. The energy and the transition strength of the low-lying collective state is quite sensitive to the cutoff energy for the RPA calculation [54]. In Fig. 2, the cutoff energy dependence of the renormalization factors and the $B(E2 \uparrow)$ value for the 2^+ state in ^{22}O are shown. Even with the cutoff energy of 70 MeV, the transition strength for the low-lying state does not converge yet. In this case, the dimension of the QRPA matrix in Eq. (3) is 11726 for the $K^\pi = 0^+$ channel and the memory size is 13 GB, and the CPU time is about 70,000s per each iteration for determining the renormalization factor f_{pp} .

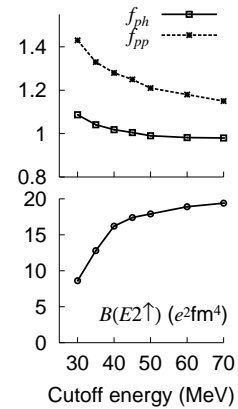


FIG. 2: Cutoff energy dependence of the renormalization factors and the $B(E2 \uparrow)$ value for the first 2^+ state in ^{22}O .

If we could perform the QRPA calculation including all quasiparticle states obtained in the HFB calculation, the renormalization factor for the pairing channel f_{pp} would be 1, because the p-p channel is treated self-consistently between the HFB and the QRPA calculations.

The peak position of the giant resonance is located slightly higher than in Ref.[49]. The non-collective two-quasiparticle states around 6 and 7 MeV are consistent between the two calculations. The energy-weighted sum ($1.867 \times 10^4 \text{ MeV} \cdot \text{fm}^4$) overestimates by about 13.9% the EWSR value ($1.638 \times 10^4 \text{ MeV} \cdot \text{fm}^4$). The overshooting of the EWSR for the isoscalar quadrupole mode in the LM approximation was pointed out in Ref [55].

IV. RESULTS AND DISCUSSION

We now discuss the properties of $^{26,28,30}\text{Ne}$ nuclei calculated with the SkM* interaction. We summarize in Table I the ground state properties of these Ne isotopes obtained by solving Eq. (1). The ground state is slightly deformed in ^{26}Ne and ^{28}Ne , and we obtain a well-deformed ground state for ^{30}Ne . The values in parentheses are experimental pairing gaps extracted by the three-point mass difference formula [44] using the experimental binding energies taken from Ref. [56]. We define the deformation parameter β_2 and average pairing gap $\langle \Delta \rangle$ [57, 58, 59, 60] as

$$\beta_2^\tau = \frac{4\pi}{5} \frac{\int d\mathbf{r} \rho^\tau(\mathbf{r}) r^2 Y_{20}(\hat{r})}{\int d\mathbf{r} \rho^\tau(\mathbf{r}) r^2}, \quad (5)$$

$$\langle \Delta_\tau \rangle = - \frac{\int d\mathbf{r} \tilde{\rho}^\tau(\mathbf{r}) \tilde{h}^\tau(\mathbf{r})}{\int d\mathbf{r} \tilde{\rho}^\tau(\mathbf{r})}, \quad (6)$$

where $\tilde{\rho}(\mathbf{r})$ is the pairing density.

Fig. 3 shows the response functions for the isovector dipole mode in neutron-rich Ne isotopes. The isovector

TABLE I: Ground state properties of $^{26,28,30}\text{Ne}$ obtained by the deformed HFB calculation with the SkM* interaction and the surface-type pairing interaction. Chemical potentials, deformations, average pairing gaps and root-mean-square radii for neutrons and protons are listed.

	^{26}Ne	^{28}Ne	^{30}Ne
λ_ν (MeV)	-4.60	-3.06	-2.90
λ_π (MeV)	-14.8	-17.0	-19.9
β_2^ν	0.08	0.12	0.32
β_2^π	0.14	0.20	0.39
$\langle \Delta_\nu \rangle$ (MeV)	0.0 (0.70)	1.27 (1.24)	1.34 (1.30)
$\langle \Delta_\pi \rangle$ (MeV)	1.04	0.87	0.0
$\sqrt{\langle r^2 \rangle}_\nu$ (fm)	3.20	3.35	3.53
$\sqrt{\langle r^2 \rangle}_\pi$ (fm)	2.93	2.98	3.08

dipole operator used in the present calculation is

$$\hat{F}_{1K} = e \frac{N}{A} \sum_i^Z r_i Y_{1K}(\hat{r}_i) - e \frac{Z}{A} \sum_i^N r_i Y_{1K}(\hat{r}_i), \quad (7)$$

and the response functions are calculated as

$$S(E) = \sum_i \sum_K \frac{\Gamma/2}{\pi} \frac{|\langle i | \hat{F}_{1K} | 0 \rangle|^2}{(E - \hbar\omega_i)^2 + \Gamma^2/4}. \quad (8)$$

A. ^{26}Ne

We can clearly see a resonance structure at around the excitation energy of 8-9 MeV, together with the giant resonance at 15–20 MeV. Because of the small deformation the K splitting is small and smeared out.

In Fig. 4, we show the transition strengths in the low-energy region. The neutron emission threshold is 6.35 MeV, and the resonance which is composed of several discrete states appears just above the threshold. In contrast to the low-lying quadrupole state in ^{22}O , the transition strengths for the dipole states in this region converge at the cutoff energy of about 40 MeV. We made a detailed analysis of the QRPA eigenmodes and show in Tables II,III the microscopic structures of the $K^\pi = 0^-$ state at 8.25 MeV and the $K^\pi = 1^-$ state at 8.76 MeV, which have the largest transition strength for each sec-

TABLE II: QRPA amplitudes for the $K^\pi = 0^-$ state in ^{26}Ne at 8.25 MeV. This mode has the proton strength $B(E1) = 2.98 \times 10^{-2} e^2 \text{fm}^2$, the neutron strength $B(Q^\nu 1) = 2.89 \times 10^{-2} e^2 \text{fm}^2$, and the isovector strength $B(Q^{\text{IV}} 1) = 1.17 \times 10^{-1} e^2 \text{fm}^2$, and the sum of backward-going amplitude $\sum |Y_{\alpha\beta}|^2 = 4.33 \times 10^{-3}$. The single-(quasi)particle levels are labeled with the asymptotic quantum numbers $[Nn_3\Lambda]\Omega$. Only components with $X_{\alpha\beta}^2 - Y_{\alpha\beta}^2 > 0.001$ are listed. Two-quasiparticle excitation energies are given by $E_\alpha + E_\beta$ in MeV and two-quasiparticle transition matrix elements $Q_{10,\alpha\beta}$ in e·fm. In the row (i), the label $\nu 1/2^-$ denotes a non-resonant discretized continuum state of neutron $\Omega^\pi = 1/2^-$ level.

	α	β	$E_\alpha + E_\beta$ (MeV)	$X_{\alpha\beta}^2 - Y_{\alpha\beta}^2$	$Q_{10,\alpha\beta}$ (e·fm)
(a)	$\nu[310]1/2$	$\nu[211]1/2$	8.15	0.670	-0.309
(b)	$\nu[330]1/2$	$\nu[220]1/2$	11.4	0.020	-0.397
(c)	$\nu[312]5/2$	$\nu[202]5/2$	11.2	0.006	-0.239
(d)	$\nu[321]3/2$	$\nu[211]3/2$	11.3	0.006	0.338
(e)	$\nu[330]1/2$	$\nu[211]1/2$	6.54	0.003	-0.118
(f)	$\nu[312]3/2$	$\nu[211]3/2$	12.8	0.002	-0.014
(g)	$\nu[301]1/2$	$\nu[211]1/2$	9.32	0.002	-0.117
(h)	$\nu[200]1/2$	$\nu[101]1/2$	14.0	0.002	-0.241
(i)	$\nu 1/2^-$	$\nu[211]1/2$	12.6	0.002	-0.068
(j)	$\pi[220]1/2$	$\pi[101]1/2$	7.96	0.265	0.0085
(k)	$\pi[330]1/2$	$\pi[220]1/2$	13.4	0.008	-0.329
(l)	$\pi[220]1/2$	$\pi[110]1/2$	14.1	0.008	-0.346

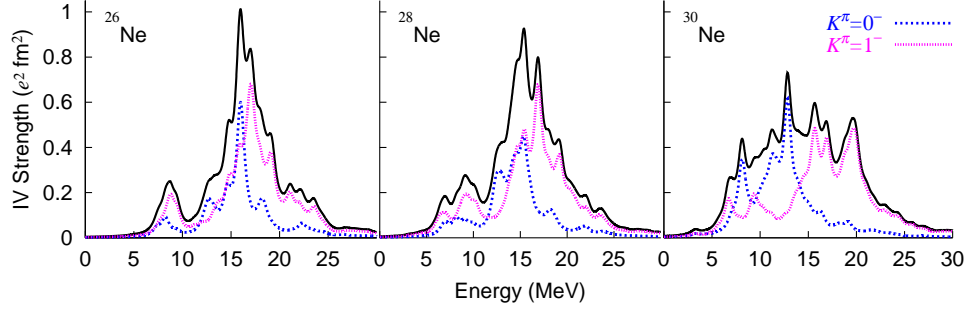


FIG. 3: Response functions for the isovector dipole operator in $^{26,28,30}\text{Ne}$. The dotted, dashed and solid lines correspond to the $K^\pi = 0^-$, $K^\pi = 1^-$ and total responses, respectively. For the $K^\pi = 1^-$ response, the transition strengths for the $K^\pi = \pm 1^-$ states are summed up. The transition strengths are smeared by using $\Gamma = 1$ MeV. The renormalization factors for the QRPA calculation are $f_{ph} = 0.919, 0.880$ and 0.929 for $^{26,28,30}\text{Ne}$ and $f_{pp} = 1.225$ for all nuclei.

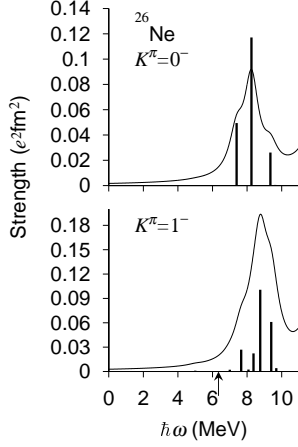


FIG. 4: Isovector dipole transition strengths in ^{26}Ne for the $K^\pi = 0^-$ (the upper) and $K^\pi = 1^-$ (the lower) states. Underlying discrete states are shown together with the smeared response functions. The arrow indicates the neutron emission threshold $E_{th} = 6.58$ MeV.

tor. In the Tables, single-(quasi)particle states are labeled with the asymptotic quantum numbers $[Nn_3\Lambda]\Omega$ just for convenience. It should be noted that the asymptotic quantum numbers are not good quantum numbers because the deformation is not so large.

For the $K^\pi = 0^-$ state at 8.25 MeV, the dominant component is the $\nu[211]1/2 \rightarrow \nu[310]1/2$ transition, corresponding to $\nu(2s_{1/2}^{-1}2p_{3/2})$. Particle-hole excitations of (b), (c) and (d) correspond to $\nu(1d_{5/2}^{-1}1f_{7/2})$ excitation, which have 3.2% contribution in total. The rows (e), (f), (g) and (h) correspond to $\nu(2s_{1/2}^{-1}1f_{7/2})$, $\nu(1d_{5/2}^{-1}2p_{3/2})$, $\nu(2s_{1/2}^{-1}2p_{1/2})$ and $\nu(1p_{1/2}^{-1}1d_{3/2})$ excitations, respectively. Two-quasiparticle proton excitations, furthermore, have an appreciable contribution; the rows (j), (k), and (l) correspond to the hole-hole like $\pi(1p_{1/2} \otimes 1d_{5/2})$ excitation, particle-hole like $\pi(1d_{5/2}^{-1}1f_{7/2})$, and $\pi(1d_{5/2}^{-1}1p_{3/2})$

TABLE III: Same as Table II but for the $K^\pi = 1^-$ state in ^{26}Ne at 8.76 MeV. This mode has $B(E1) = 1.65 \times 10^{-2} e^2 \text{fm}^2$, $B(Q^{\nu}1) = 3.58 \times 10^{-2} e^2 \text{fm}^2$, $B(Q^{\text{IV}}1) = 1.00 \times 10^{-1} e^2 \text{fm}^2$, and $\sum |Y_{\alpha\beta}|^2 = 2.93 \times 10^{-3}$.

	α	β	$E_\alpha + E_\beta$ (MeV)	$X_{\alpha\beta}^2 - Y_{\alpha\beta}^2$	$Q_{11,\alpha\beta}$ (e · fm)
(a)	$\nu[312]3/2$	$\nu[211]1/2$	8.68	0.849	0.339
(b)	$\nu[310]1/2$	$\nu[211]1/2$	8.16	0.040	-0.131
(c)	$\nu[301]1/2$	$\nu[211]1/2$	9.32	0.010	0.294
(d)	$\nu[321]3/2$	$\nu[220]1/2$	12.0	0.007	0.250
(e)	$\nu[303]7/2$	$\nu[202]5/2$	12.1	0.006	0.414
(f)	$\nu[330]1/2$	$\nu[220]1/2$	11.4	0.004	-0.127
(g)	$\nu[312]5/2$	$\nu[211]3/2$	12.1	0.004	0.348
(h)	$\nu[321]3/2$	$\nu[202]5/2$	10.3	0.001	-0.010
(i)	$\nu[321]3/2$	$\nu[202]5/2$	11.8	0.003	-0.214
(j)	$\nu[330]1/2$	$\nu[211]1/2$	6.54	0.003	-0.081
(k)	$\nu[321]3/2$	$\nu[211]1/2$	7.14	0.001	0.106
(l)	$\pi[220]1/2$	$\pi[101]1/2$	7.96	0.037	0.0095
(m)	$\pi[211]3/2$	$\pi[101]1/2$	7.95	0.015	-0.011
(n)	$\pi[321]3/2$	$\pi[220]1/2$	14.0	0.004	0.313
(o)	$\pi[312]5/2$	$\pi[211]3/2$	14.7	0.002	-0.338
(p)	$\pi[211]3/2$	$\pi[110]1/2$	14.1	0.002	0.280
(q)	$\pi[211]1/2$	$\pi[101]1/2$	11.5	0.002	-0.256

excitations, respectively. The $K^\pi = 1^-$ state has a similar structure to the $K^\pi = 0^-$ state. The main component is $\nu(2s_{1/2}^{-1}2p_{3/2})$, which corresponds to (a) and (b) in Table III. With a small contribution, many other neutron particle-hole and proton two-quasiparticle excitations build the excitation mode at 8.76 MeV. The resonance is also composed of the $K^\pi = 1^-$ mode appearing at 9.40 MeV. This mode is dominantly (97.6%) generated by the $\nu[211]1/2 \rightarrow \nu[301]1/2$ transition corresponding to the $\nu(2s_{1/2}^{-1}2p_{1/2})$ transition.

Preliminary calculations of deformed QRPA using the Gogny interaction [61], and the relativistic deformed QRPA [62] show that the low-lying dipole state is dominantly constructed by the $\nu(2s_{1/2}^{-1}2p_{3/2})$ configuration.

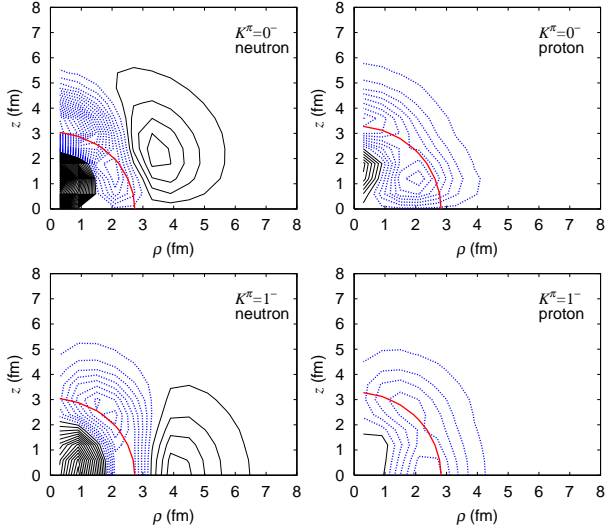


FIG. 5: Transition densities in ^{26}Ne for the $K^\pi = 0^-$ state at 8.25 MeV (upper panels), and for the $K^\pi = 1^-$ state at 8.76 MeV (lower panels). Solid and dotted lines indicate positive and negative transition densities, and the contour lines are plotted at intervals of $3 \times 10^{-4} \text{ fm}^{-3}$. The thick solid lines indicate the neutron and proton half density, 0.058 fm^{-3} and 0.036 fm^{-3} , respectively.

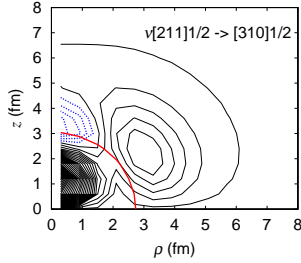


FIG. 6: Same as Fig. 5, for the unperturbed transition density of $\nu[211]1/2 \rightarrow [310]1/2$ excitation.

In Fig. 5, we show transition densities for the $K^\pi = 0^-$ state at 8.25 MeV, and for the $K^\pi = 1^-$ state at 8.76 MeV. These transition densities are quite different from the classical picture of the isovector giant resonances. They have an isoscalar character in the surface region of the nucleus. On the other hand, outside of the nucleus, neutrons have an oscillation and the neutron excitation is dominant. Furthermore, the neutron excitations take place in the low-density region around 6 fm, namely, this mode has a unique picture of vibration of the neutron skin. The spatially extended structure of the $\nu[211]1/2$ state is responsible for this tail of the neutron transition density. In order to clearly see the spatial structure of $\nu[211]1/2$, the unperturbed transition density of $\nu[211]1/2 \rightarrow [310]1/2$ is shown in Fig. 6. It is clear that the wave function extends far outside of the nucleus, and the extension is larger than in the dipole state of Fig. 5.

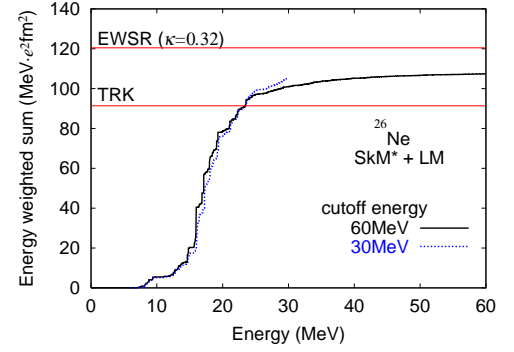


FIG. 7: Energy weighted sum of the isovector dipole strength function. The solid and the dotted lines are calculations with the energy cutoff at 60 and 30 MeV. The horizontal lines show the classical TRK, and the RPA sum rule including the enhancement factor, $m_1 = m_1^{\text{cl}}(1 + \kappa)$. Here $\kappa = 0.32$ for the SkM* interaction in ^{26}Ne .

Furthermore, the structure around the surface is different between the unperturbed one and that obtained in the QRPA. These differences are generated by the QRPA correlations; the low-lying dipole state possesses a collective nature, which is small but finite.

Fig. 7 shows the energy weighted sum of the isovector dipole strength function together with the sum rule values represented by the horizontal lines. The calculated sum satisfies 89.2% of the EWSR value including the enhancement factor κ ; $m_1 = m_1^{\text{cl}}(1 + \kappa)$ [26]. The enhancement factor comes from the momentum dependence of the Skyrme density functionals. The effect of the explicit treatment of the momentum dependence for the EWSR was discussed in the discretized-continuum QRPA [63] and the continuum QRPA [55] for the spherical systems. In the present calculation, we treat the momentum dependence in the LM approximation. Therefore, discrepancy between the calculation and the EWSR value comes from this treatment of the momentum dependence. This point remains to be improved, and it is discussed in Ref. [64].

In the present calculation, the energy-weighted sum up to 10 MeV is $5.51 \text{ MeV} \cdot e^2 \text{ fm}^2$, corresponding to 6.0% of the TRK sum-rule value, 4.6% of the EWSR including the enhancement factor and 5.1% of the calculated sum. These values are consistent with the experiment [34]. In Fig. 7, we also show the energy-weighted sum calculated with the energy cutoff at 30 MeV (dotted line). In the giant resonance region, two calculations give different results, while they are almost identical in the low-energy region. This is because the collectivity of the low-lying resonance is small, and consequently the transition strength is not very sensitive to the cutoff energy.

Before going to the neighboring nuclei, it should be noted that we obtain the collective octupole state at about 5.2 MeV, below the neutron threshold, with $B(E3 \uparrow) = 2458 e^2 \text{ fm}^6$, which corresponds to about 61 in Weisskopf units and the isoscalar

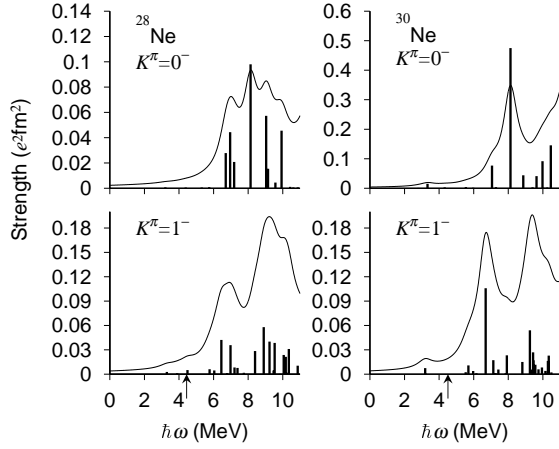


FIG. 8: Same as Fig. 4 but for ^{28}Ne and ^{30}Ne . The arrows indicate the neutron emission threshold $E_{\text{th}} = 4.44$ and 4.51 MeV.

transition strength is $2.60 \times 10^4 \text{fm}^6$. The lowest $K^\pi = 0^-$ state is located at 5.03 MeV and the sum of the backward-going amplitudes is 0.099 . This state is generated by $\nu[211]1/2 \rightarrow [330]1/2(53.2\%)$, $\nu[202]5/2 \rightarrow [312]5/2(6.8\%)$, $\nu[211]1/2 \rightarrow [310]1/2(6.5\%)$, $\nu[220]1/2 \rightarrow [330]1/2(3.7\%)$, and $\pi[101]2/1 \otimes [220]1/2(14.8\%)$, $\pi[101]3/2 \otimes [211]3/2(2.2\%)$, $\pi[220]1/2 \otimes [330]1/2(2.1\%)$, $\pi[101]1/2 \otimes [211]1/2(1.0\%)$.

B. ^{28}Ne and ^{30}Ne

The central panel in Fig. 3 shows the response function in ^{28}Ne . In the low-energy region, we can see a two-bump structure at around 7 and 8 MeV. Because the deformation is small as in ^{26}Ne , we cannot see a splitting of the giant resonance. In Fig. 8, we show the low-energy part of the strength functions. In the $K^\pi = 0^-$ states, there is a prominent peak at 8.1 MeV with a strength of $0.098 \text{e}^2\text{fm}^2$. The strength distribution is fragmented for the $K^\pi = 1^-$ mode, but correspondingly, we can see an eigenmode at 8.9 MeV with the largest transition strength of $0.058 \text{e}^2\text{fm}^2$.

We show in Table IV the QRPA amplitude for the $K^\pi = 0^-$ state at 8.14 MeV in ^{28}Ne . The main component is the neutron two-quasiparticle excitation of $\nu([310]1/2 \otimes [211]1/2)$ corresponding to $\nu(2s_{1/2}^{-1}2p_{3/2})$. Two quasiparticle excitations of (b) and (c) in Table IV correspond to $\nu(1d_{5/2}^{-1}1f_{7/2})$, and (d): $\nu(2s_{1/2}^{-1}1f_{7/2})$, (e) and (f): $\nu(1d_{3/2}^{-1}2p_{3/2})$, (g): $\nu(1d_{3/2}^{-1}1f_{7/2})$, (h) and (i): $\nu(1d_{5/2}^{-1}2p_{3/2})$, and (j): $\nu(1d_{5/2}^{-1}2p_{1/2})$ excitations, respectively. The proton excitation of $\pi(1p_{1/2} \otimes 1d_{5/2})$ has an appreciable contribution as in ^{26}Ne .

The lower energy resonance at around 7 MeV is described by three eigenstates as shown in Fig. 8. The lower state at 6.70 MeV, which has an isovector strength

TABLE IV: Same as Table II but for the $K^\pi = 0^-$ state at 8.14 MeV in ^{28}Ne . This mode has $B(E1) = 2.62 \times 10^{-2} \text{e}^2\text{fm}^2$, $B(Q^{\text{IV}}1) = 2.29 \times 10^{-2} \text{e}^2\text{fm}^2$, $B(Q^{\text{IV}}1) = 9.80 \times 10^{-2} \text{e}^2\text{fm}^2$, and $\sum |Y_{\alpha\beta}|^2 = 9.77 \times 10^{-3}$. In the rows (k), (l), (m), (n) and (t), the labels $\nu 1/2^-$, $\nu 1/2^+$ and $\pi 1/2^+$ denote non-resonant discretized continuum states of neutron $\Omega^\pi = 1/2^-$ and $1/2^+$ levels and proton $1/2^+$ level.

		$E_\alpha + E_\beta$ (MeV)	$X_{\alpha\beta}^2 - Y_{\alpha\beta}^2$	$Q_{10,\alpha\beta}$ (e · fm)
α	β			
(a)	$\nu[310]1/2 \ \nu[211]1/2$	8.27	0.569	-0.303
(b)	$\nu[330]1/2 \ \nu[220]1/2$	11.2	0.055	-0.373
(c)	$\nu[321]3/2 \ \nu[211]3/2$	10.9	0.006	0.323
(d)	$\nu[330]1/2 \ \nu[211]1/2$	6.20	0.036	-0.096
(e)	$\nu[312]3/2 \ \nu[202]3/2$	6.82	0.004	-0.039
(f)	$\nu[310]1/2 \ \nu[200]1/2$	5.81	0.003	0.026
(g)	$\nu[330]1/2 \ \nu[200]1/2$	3.74	0.004	-0.006
(h)	$\nu[321]3/2 \ \nu[211]3/2$	12.9	0.002	-0.014
(i)	$\nu[310]1/2 \ \nu[220]1/2$	13.3	0.001	0.0004
(j)	$\nu[301]1/2 \ \nu[220]1/2$	14.5	0.001	-0.022
(k)	$\nu 1/2^- \ \nu[200]1/2$	10.1	0.009	0.203
(l)	$\nu 1/2^- \ \nu[202]3/2$	10.7	0.002	0.099
(m)	$\nu 1/2^- \ \nu[211]1/2$	12.6	0.004	-0.071
(n)	$\nu 1/2^+ \ \nu[330]1/2$	14.2	0.003	-0.114
(o)	$\pi[220]1/2 \ \pi[101]1/2$	7.63	0.238	0.018
(p)	$\pi[330]1/2 \ \pi[220]1/2$	12.8	0.031	-0.463
(q)	$\pi[220]1/2 \ \pi[110]1/2$	13.7	0.007	-0.441
(r)	$\pi[211]3/2 \ \pi[101]3/2$	12.3	0.004	-0.310
(s)	$\pi[211]1/2 \ \pi[101]1/2$	11.6	0.002	0.288
(t)	$\pi 1/2^- \ \pi[220]1/2$	19.3	0.001	0.004

of $0.028 \text{e}^2\text{fm}^2$, is mainly generated by $\nu(1d_{3/2}^{-1}2p_{3/2})$ (87.5%), $\nu(2s_{1/2}^{-1}1f_{7/2})$ (5.7%) and $\nu(1d_{3/2}^{-1}2p_{1/2})$ (2.4%). The state at 6.96 MeV with $B(Q^{\text{IV}}1) = 0.044 \text{e}^2\text{fm}^2$ is almost a single p-h excitation of $\nu(1d_{3/2}^{-1}2p_{1/2})$ (90.2%), and the state at 7.19 MeV with $0.021 \text{e}^2\text{fm}^2$ is generated dominantly by proton h-h like excitation of $\pi(1p_{1/2} \otimes 1d_{5/2})$ (57.8%), together with $\nu(2s_{1/2}^{-1}1f_{7/2})$ (18.6%), $\nu(1d_{3/2}^{-1}2p_{3/2})$ (6.4%), $\nu(1d_{5/2}^{-1}1f_{7/2})$ (5.2%), $\nu(2s_{1/2}^{-1}2p_{3/2})$ (4.5%) and $\nu(1d_{3/2}^{-1}2p_{1/2})$ (1.8%).

Therefore, the higher-energy resonance at 8 MeV has a similar structure to that in ^{26}Ne ; $\nu(2s_{1/2}^{-1}2p_{3/2})$ and $\pi(1p_{1/2} \otimes 1d_{5/2})$ excitations are dominant, and the lower-energy resonance is generated by different eigenmodes.

The $K^\pi = 1^-$ state at 8.9 MeV in ^{28}Ne has a similar structure to that in ^{26}Ne and $K^\pi = 0^-$ state in ^{28}Ne , corresponding mainly to the neutron two-quasiparticle excitation of $\nu(2s_{1/2}^{-1}2p_{3/2})$, with 64.0% contribution. In addition to this neutron p-h like excitation, the following excitations have an appreciable contribution; $\nu(1d_{5/2}^{-1}1f_{7/2})$ (13.9%), $\nu(2s_{1/2}^{-1}1f_{7/2})$ (2.8%), $\pi(1p_{1/2} \otimes 1d_{5/2})$ (7.9%) and $\pi(1p_{3/2} \otimes 1d_{5/2})$ (1.4%).

Finally, we discuss the dipole state in ^{30}Ne . Compared to the response functions in ^{26}Ne and ^{28}Ne , that for ^{30}Ne is quite different, because this nucleus is well deformed

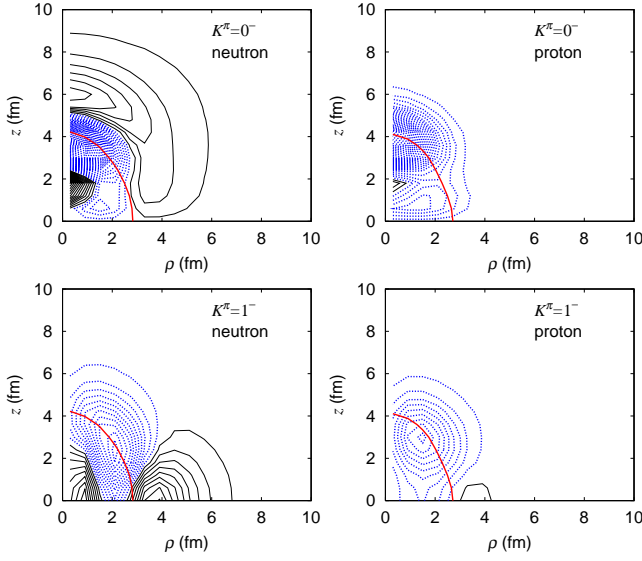


FIG. 9: Same as Fig. 5 but for the $K^\pi = 0^-$ state at 8.1 MeV and for the $K^\pi = 1^-$ state at 6.7 MeV in ^{30}Ne .

as shown in Table I. The giant resonance is split into $K^\pi = 0^-$ and 1^- mode, and the split giant resonance has an overlap with the low-lying resonance below 10 MeV. In the right panel of Fig. 8, we show the strength distribution below 10 MeV in ^{30}Ne . For the $K^\pi = 0^-$ mode, we can see a prominent peak at 8.1 MeV possessing a large isovector $E1$ strength of $0.48 e^2\text{fm}^2$. This state is mainly generated by $\nu[211]1/2 \rightarrow [310]1/2$ (38.4%) and the neutron excitation from $[330]1/2$ to the non-resonance continuum state (37.9%), together with the proton excitation of $\pi[330]1/2 \rightarrow [220]1/2$ (6.1%).

In Fig. 9, the transition density for the $K^\pi = 0^-$ state is shown. The transition density of protons are quite similar to that in Fig. 5. For the neutrons, we can easily see the effect of mixing of the excitation into the continuum state; the transition density has large spatial extension. Furthermore, comparing to Fig. 6, this $K^\pi = 0^-$ state still possesses a structure similar to the low-lying dipole state in ^{26}Ne .

For the $K^\pi = 1^-$ state, we can see a prominent peak at 6.69 MeV possessing an isovector strength of $0.11 e^2\text{fm}^2$. This state has a different structure to the dipole states discussed above. In Table V, we show its microscopic structure. This state has a collective nature in a sense that a number of two-quasiparticle excitations have an appreciable contribution; in the present case, eight of the neutron excitations have a contribution larger than 1%. In the lower panel of Fig. 9, the transition density of this state is shown. This mode has also a characteristic feature that the neutron and proton contribution have an isoscalar nature around the surface region, and the neutron excitation is dominant outside of the nucleus.

It is difficult to link directly with the low-lying dipole states in ^{26}Ne or ^{28}Ne , because the deformations are quite

TABLE V: Same as Table II but for the $K^\pi = 1^-$ state at 6.69 MeV in ^{30}Ne , and only components with $X_{\alpha\beta}^2 - Y_{\alpha\beta}^2 > 0.01$ are listed. This mode has $B(E1) = 1.58 \times 10^{-2} e^2\text{fm}^2$, $B(Q^{\nu}1) = 3.98 \times 10^{-2} e^2\text{fm}^2$, $B(Q^{\text{IV}}1) = 1.06 \times 10^{-1} e^2\text{fm}^2$, and $\sum |Y_{\alpha\beta}|^2 = 8.82 \times 10^{-3}$.

		$E_\alpha + E_\beta$		$Q_{11,\alpha\beta}$
α	β	(MeV)	$X_{\alpha\beta}^2 - Y_{\alpha\beta}^2$	
(a)	$\nu[312]3/2 \rightarrow \nu[200]1/2$	6.87	0.676	0.207
(b)	$\nu[310]1/2 \rightarrow \nu[200]1/2$	7.09	0.089	0.141
(c)	$\nu[321]3/2 \rightarrow \nu[202]5/2$	7.52	0.043	-0.009
(d)	$\nu[321]3/2 \rightarrow \nu[211]1/2$	5.72	0.038	0.026
(e)	$\nu[312]5/2 \rightarrow \nu[202]3/2$	6.16	0.025	0.003
(f)	$\nu[310]1/2 \rightarrow \nu[202]3/2$	6.13	0.025	0.015
(g)	$\nu[330]1/2 \rightarrow \nu[211]1/2$	5.73	0.011	0.040
(h)	$\nu 1/2^- \rightarrow \nu[202]3/2$	7.57	0.019	0.066

different in ^{30}Ne and in the other two nuclei. The main component of this $K^\pi = 1^-$ state is (a): $\nu[200]1/2 \rightarrow [312]3/2$ and (b): $\nu[200]1/2 \rightarrow [310]1/2$. These p-h excitations are $\nu(1d_{3/2}^{-1}2p_{3/2})$ in the spherical limit. In this sense, the lower-energy resonance in ^{28}Ne is connected to this collective $K^\pi = 1^-$ state in ^{30}Ne .

V. SUMMARY

We have investigated a new framework of the deformed QRPA based on the Skyrme density functionals and the Landau-Migdal approximation. With this method, we have made a detailed analysis of the low-lying dipole states in neutron-rich $^{26,28,30}\text{Ne}$. In these nuclei, we obtain the excitation mode at 8 – 8.5 MeV. The low-lying resonance is composed of several QRPA eigenmodes. In ^{26}Ne , not only the $\nu(2s_{1/2}^{-1}2p_{3/2})$ transition but also the $\nu(2s_{1/2}^{-1}2p_{1/2})$ transition contribute to generating the resonance. In ^{28}Ne and ^{30}Ne , the $\nu[211]1/2 \rightarrow [310]1/2$ excitation still plays a major role. Each eigenmode is, however, not purely a single particle-hole excitation, it has a small contribution of the other neutron excitations and proton excitations as well.

We have clearly shown the spatially extended structure of the $\nu[211]1/2$ ($2s_{1/2}$) state, and that it is responsible for the oscillation of transition density of neutrons outside of the nucleus. In the well deformed nucleus ^{30}Ne , the deformation splitting of the giant resonance is large and the low-lying resonance overlaps with the giant resonance. For the $K^\pi = 1^-$ state, we furthermore obtain a collective dipole mode at 6.7 MeV.

Acknowledgments

The authors thank D. Beaumel, L. G. Cao and members of the Groupe Théorie in IPN Orsay for useful dis-

cussions and comments. One of the authors (K.Y) is supported by Research Fellowships of the Japan Society for the Promotion of Science for Young Scientists. This work was supported by the JSPS Core-to-Core Program “International Research Network for Exotic Femto Sys-

tems”. The numerical calculations were performed on the NEC SX-8 supercomputers at Yukawa Institute for Theoretical Physics, Kyoto University and at Research Center for Nuclear Physics, Osaka University.

-
- [1] I. Tanihata (Ed), Nucl. Phys. **A693**, Nos. 1, 2 (2001).
 - [2] H. Horiuchi, T. Otsuka, Y. Suzuki (Eds.), Prog. Theor. Phys. Suppl. No.142 (2001).
 - [3] K. Hagino, H. Horiuchi, M. Matsuo, I. Tanihata (Eds.), Prog. Theor. Phys. Suppl. No.146 (2002).
 - [4] P. von Neumann-Cosel and T. Aumann (Eds.), Nucl. Phys. **A788**, (2007).
 - [5] T. Suzuki *et al.*, Phys. Rev. Lett. **75**, 3241 (1995).
 - [6] S. Mizutori, J. Dobaczewski, G. A. Lalazissis, W. Nazarewicz, and P.-G. Reinhard, Phys. Rev. C **61**, 044326 (2000), and references therein.
 - [7] K. Ikeda, Nucl. Phys. **A538**, 355c (1992).
 - [8] D. Sackett *et al.*, Phys. Rev. C **48**, 118 (1993).
 - [9] S. Shimoura *et al.*, Phys. Lett. **B348**, 29 (1995).
 - [10] M. Zinser *et al.*, Nucl. Phys. **A619**, 151 (1997).
 - [11] T. Nakamura *et al.*, Phys. Rev. Lett. **96**, 252502 (2006).
 - [12] T. Nakamura *et al.*, Phys. Lett. **B331**, 296 (1994).
 - [13] R. Palit *et al.*, Phys. Rev. C **68**, 034318 (2003).
 - [14] N. Fukuda *et al.*, Phys. Rev. C **70**, 054506 (2004).
 - [15] T. Nakamura *et al.*, Phys. Phys. Lett. **83**, 1112 (1999).
 - [16] U. D. Pramanik *et al.*, Phys. Lett. **B551**, 63 (2003).
 - [17] T. Aumann *et al.*, Phys. Rev. C **59**, 1252 (1999).
 - [18] A. Leistenschneider *et al.*, Phys. Rev. Lett. **86**, 5442 (2001).
 - [19] E. Tryggestad *et al.*, Phys. Rev. C **67**, 064309 (2003).
 - [20] P. Adrich *et al.*, Phys. Rev. Lett. **95**, 132501 (2005).
 - [21] F. Catara, E. G. Lanza, M. A. Nagarajan, and A. Vitturi, Nucl. Phys. **A624**, 449 (1997).
 - [22] I. Hamamoto, H. Sagawa, and X. Z. Zhang, Phys. Rev. C **57**, R1064 (1998).
 - [23] I. Hamamoto, H. Sagawa, and X. Z. Zhang, Nucl. Phys. **A648**, 203 (1999).
 - [24] S. Goriely and E. Khan, Nucl. Phys. **A706**, 217 (2002).
 - [25] M. Matsuo, Prog. Theor. Phys. Suppl. **146**, 110 (2002).
 - [26] J. Terasaki, J. Engel, Phys. Rev. C **74**, 044301 (2006).
 - [27] G. Colò, P. F. Bortignon, Nucl. Phys. **A696**, 427 (2001).
 - [28] D. Sarchi, P. F. Bortignon and G. Colò, Phys. Lett. **B601**, 27 (2004).
 - [29] D. Vretenar, N. Paar, P. Ring, G. A. Lalazissis, Phys. Rev. C **63**, 047301 (2001).
 - [30] D. Vretenar, N. Paar, P. Ring, G. A. Lalazissis, Nucl. Phys. **A692**, 496 (2001).
 - [31] N. Paar, T. Nikšić, D. Vretenar, P. Ring, Phys. Lett. **B606**, 288 (2005).
 - [32] L. G. Cao, Z. Y. Ma, Phys. Rev. C **71**, 034305 (2005).
 - [33] E. Litvinova, P. Ring, and D. Vretenar, Phys. Lett. **B647**, 111 (2007).
 - [34] J. Gibelin *et al.*, Nucl. Phys. **A788**, 153c (2007).
 - [35] E. Khan, N. Sandulescu, and N. Van Giai, Phys. Rev. C **71** (2005) R042801.
 - [36] K. Yoshida, M. Yamagami, K. Matsuyanagi, Nucl. Phys. **A779**, 99 (2006).
 - [37] A. Bulgac, Preprint No. FT-194-1980, Institute of Atomic Physics, Bucharest, 1980. [arXiv:nucl-th/9907088]
 - [38] J. Dobaczewski, H. Flocard and J. Treiner, Nucl. Phys. **A422**, 103 (1984).
 - [39] J. Bartel, P. Quentin, M. Brack, C. Guet, and H.-B. Håkansson, Nucl. Phys. **A386**, 79 (1982).
 - [40] E. Terán, V. E. Oberacker and A. S. Umar, Phys. Rev. C **67**, 064314 (2003).
 - [41] M. V. Stoitsov, J. Dobaczewski, W. Nazarewicz, P. Ring, Comp. Phys. Comm. **167**, 43 (2005).
 - [42] G. F. Bertsch, H. Esbensen, Ann. Phys. **209**, 327 (1991).
 - [43] J. Terasaki, P.-H. Heenen, P. Bonche, J. Dobaczewski, H. Flocard, Nucl. Phys. **A593**, 1 (1995).
 - [44] W. Satuła, J. Dobaczewski, and W. Nazarewicz, Phys. Rev. Lett. **81**, 3599 (1998).
 - [45] D. J. Rowe, *Nuclear Collective Motion*, (Methuen and Co. Ltd., 1970).
 - [46] S. O. Bäckman, A. D. Jackson, and J. Speth, Phys. Lett. **B56**, 209 (1975).
 - [47] N. Van Giai and H. Sagawa, Phys. Lett. **B106**, 379 (1981).
 - [48] N. Van Giai, Ch. Stoyanov, V. V. Voronov, Phys. Rev. C **57**, 1204 (1998).
 - [49] E. Khan, N. Sandulescu, M. Grasso, N. Van Giai, Phys. Rev. C **66**, 024309 (2002).
 - [50] E. Chabanat, P. Bonche, P. Haensel, J. Meyer, and R. Schaeffer, Nucl. Phys. **A635**, 231 (1998).
 - [51] M. Bellguic, *et al.*, Nucl. Phys. **A682**, 136c (2001).
 - [52] P. G. Thirolf, *et al.*, Phys. Lett. **B485**, 16 (2000).
 - [53] E. Becheva, *et al.*, Phys. Rev. Lett. **96**, 012501 (2006).
 - [54] J.-P. Blaizot and D. Gogny, Nucl. Phys. **A284**, 429 (1977).
 - [55] K. Mizuyama, M. Matsuo and Y. Serizawa, arXiv:0706.1115.
 - [56] G. Audi and A. H. Wapstra, Nucl. Phys. **A461**, 322 (1995).
 - [57] J. Sauvage-Letessier, P. Quentin, H. Flocard, Nucl. Phys. **A370**, 231 (1981).
 - [58] M. Bender, K. Rutz, P.-G. Reinhard, J. A. Maruhn, Eur. Phys. J. A **8**, 59 (2000).
 - [59] T. Duguet, P. Bonche, P.-H. Heenen, Nucl. Phys. **A679**, 427 (2001).
 - [60] M. Yamagami, K. Matsuyanagi, M. Matsuo, Nucl. Phys. **A693**, 579 (2001).
 - [61] S. Péru, H. Goutte, J. F. Berger, Nucl. Phys. **A788**, 44c (2007).
 - [62] D. Peña Arteaga, and P. Ring, Prog. Part. Nucl. Phys. **59**, 314 (2007).
 - [63] M. Yamagami, E. Khan, and N. Van Giai, in *Proceedings of the International Symposium on Frontiers of Collective Motions (CM2002)* (World Scientific, Singapore, 2002).
 - [64] K. Yoshida, in preparation.